Journal of Membrane Science 643 (2022) 120020

Contents lists available at ScienceDirect

Journal of Membrane Science

journal homepage: www.elsevier.com/locate/memsci

Chemical physics insight of PPy-based modified ion exchange membranes: A fundamental approach

I. Salmeron-Sanchez [a,*], J. Asenjo-Pascual [a], J.R. Avilés-Moreno [a], J.C. Pérez-Flores [b], P. Mauleón [c], P. Ocón [a]

[a] Universidad Autónoma de Madrid (UAM), Departamento de Química Física Aplicada, C/Francisco Tomás y Valiente 7, 28049, Madrid, Spain
[b] Instituto de Investigación de Energías Renovables, Universidad de Castilla-La Mancha, C/Investigación 1, Edif. 3, 02071, Albacete, Spain
[c] Universidad Autónoma de Madrid (UAM), Departamento de Química Orgánica, C/Francisco Tomás y Valiente 7, 28049, Madrid, Spain

ARTICLE INFO

Keywords:
Ion exchange membrane
Membrane modification
Permeability
Permselectivity
Mechanical properties

ABSTRACT

Four commercially available, cost-effective ion exchange membranes (two cationic and two anionic exchange membranes, CEMs and AEMs, respectively) were modified to mitigate crossover phenomena of the redox active species typically observed in Aqueous Organic Redox Flow Batteries (AORFB) systems. The modification strategy was carried out using a pyrrole(Py)-based polymer which successfully reduced the permeation of two redox active organic molecules, a viologen derivative (named BP7 throughout this study) and TEMPOL, by an order of magnitude. Additionally, modified membranes showed not significant changes in ion conductivity, with negligible effect on the electrical conductivity of the membranes at a given conditions. The morphology, physicochemical, mechanical, and electrochemical properties of the membranes were determined to evaluate the impact of these modifications. AEMs modified in this manner were found to have optimal properties, showing an increase in ion exchange capacity while maintaining excellent mechanical stability and unaltered permselectivity. Additionally, the diffusion boundary layer of these AEMs was slightly extended, which suggests a greater double layer stability for ion exchange processes than in the case of CEMs. Our work shows that these modified membranes could be an appealing approach for AORFB applications.

1. Introduction

Redox Flow Batteries (RFBs) have been a major research interest as a large-scale electrical energy storage system due to their well-known ability for the efficient utilization of renewable energy. In particular, all-vanadium RFBs [1] have been considered the quintessential system for energy storage applications. However, their elevated cost compromises their long-term economic viability. In an effort to decrease the cost of RFBs and improve their applicability, the HIGREEW (*Affordable High-performance Green Redox Flow Batteries*) project was created to provide solutions to these issues by looking at redox active organic molecules as aqueous and neutral electrolytes for Aqueous Organic Redox Flow Batteries (AORFB). One of the redox couples that have been considered in the project are methyl viologen derivative 7,8-dihydro-6H-dipyrido[1,2-a:2′,1′-c] [1,2]diazepine-5,9-diium dibromide, henceforth BP7 as anolyte [3], and TEMPOL (4-hydroxy-2,2,6,6-tetramethylpiperidin-1-oxyl) as catholyte [4] due to the remarkable electrochemical properties of this pair. The energy of the AORFB is carried by charging the BP7 from +2 to +1 cation, while the neutral TEMPOL is oxidized to a singly charged cation. The energy is interconverted between the electrical and electrochemical form by the battery cell or stack, where one of the key components is the membrane electrode assembly.

Up to now, Nafion® ionomer is the most used ion exchange membrane for energy-related electrochemical devices which require high efficiency and energy density, as well as long term chemical stability under changing oxidant conditions [2,5–8]. However, Nafion® is an expensive material and exhibits crossover phenomena of redox active species which limits its extensive application in electrochemical devices such as RFBs [9]. Prior to assess the potential use of a membrane in RFB devices, it must exhibit high ionic selectivity and conductivity towards counter-ions. Additionally, in the presence of significant crossover phenomena the capacity of the battery is diminished, which ultimately results in self-discharge. Therefore, an ideal membrane should offer the following characteristics: good chemical and mechanical stability, high conductivity, low permeability to redox-active species whereas high

* Corresponding author.
E-mail address: ivan.salmeron@uam.es (I. Salmeron-Sanchez).

https://doi.org/10.1016/j.memsci.2021.120020
Received 5 July 2021; Received in revised form 22 October 2021; Accepted 27 October 2021
Available online 3 November 2021

permselectivity to the charge carriers of the electrolyte solution, low cost, and low transfer of water from one compartment cell to the other.

There are several strategies [10–13] that can be used to improve the properties of ion exchange membranes such as the additive incorporations to yield specific properties, the surface modifications and the performance improvement in terms of permeability. However, most of these modifications cause loss in its conductivity [14] which would have a bigger impact on the VE.

In this work, we have explored the immersion of the membrane in polymerized pyrrole (Py) as an alternative strategy for efficient membrane modification. This approach has been previously applied to Nafion® in VRFBs [15] showing that polypyrrole (PPy) attached to the membrane enhances the properties of ion exchange membranes. PPy exhibits appreciable ion conductivity in the oxidized state [16] and, depending on the doping level, the electronic conductivity is higher when the polymerization is performed electrochemically. Also, the methodology is environmentally friendly compared with others procedures based on the organic solvents, e.g. the case of nitromethane [17].

The effect of incorporating another material to the matrix polymer of a membrane changes the microstructure of the membranes [18], which may lead to different behaviour in terms of physicochemical, electrical, and mechanical properties [19–21]. The permselectivity may also differ since the hydrophilic channels and exchangeable sites of the composite are affected as well. Thus, ion transport is another element of interest for our work.

Here, four commercially available, cost-effective ion exchange membranes (two CEMs and two AEMs) alternative to Nafion® were tested to evaluate their physicochemical, ion transport properties, and electrochemical behaviour before and after membrane modification to determine the impact on membrane properties. Thus, water uptake, ion exchange capacity, ion conductivity, mechanical properties, contact angle and transport number, permselectivity as well as the electrical response of membrane by chronopotentiometry have been studied and determined. Furthermore, we introduce a characterization technique for PPy modification of ion exchange membranes that provides a deeper knowledge of the architecture of these materials, and hence insight into their potential application in RFBs.

2. Experimental section

2.1. Materials

FAA-3-50, FAA-3-PE-30, FS-950 and E-630(K) membranes were purchased from Fumatech BWT Company. Sodium chloride (99.90%) was purchased from Aldo. Sulphuric acid (95–98 % wt) and hexahydrate iron chloride(III) (98%) were purchased from Panreac. Pyrrole (98%) was provided from Sima-Aldrich (Merck) and was previously distilled before use. TEMPOL was purchased from Glentham Life Science and BP7 was synthetized following the procedure as described in SI (Fig. S1 and S2).

2.2. Membrane pre-treatment

The as-received Fumatech membranes were all soaked in NaCl 1 M solution to promote the exchange of the desired counter-ions. Vertical rotating agitation (Intelli mixer) was held for 24 h minimum at room temperature. Finally, they are stored in NaCl 1 M before use. The membranes selected in this work are under patent protection. As consequence, we have performed an extensive characterization to find out as much as possible about the chemical structure of the membranes.

2.3. Preparation of modified membranes

Modification of pre-treated commercial membranes were done via chemical *in situ* polymerization, as depicted in Fig. 1. Polymerization

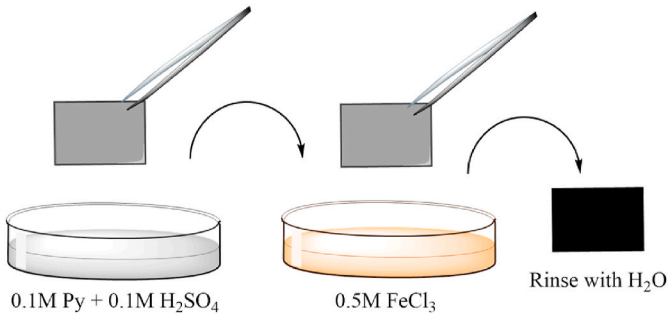

Fig. 1. Scheme of membrane modification procedure.

process was developed by soaking the corresponding membrane into a 1:1 Pyrrole (Py) 0.1 M and H_2SO_4 0.1 M solution for 6 min. After that, membrane was immersed in another solution containing the oxidant for 18 min ($FeCl_3{\cdot}6H_2O$, in this work). Afterwards, membranes were rinsed out using DI water and stored in NaCl 1 M. As obtained, membranes were denoted as substrate-PPy, where PPy means polypyrrole.

2.4. Morphology and optical analysis

2.4.1. SEM and elemental analysis

Morphology of the membrane surface and cross-section was observed using a Hitachi S-300 scanning electron microscope (SEM). The membrane samples were investigated in dried conditions. The water was removed using vacuum oven at 60 °C at 100 mbar for overnight (Memmert Vacuum drying oven VO) and then stored in vacuum before analysis. Membranes were coated with a thin gold layer under vacuum once was clamped in a brass holder. The elemental analysis was determined with an INCAxsight (Oxford Instruments) energy-dispersive X-ray spectroscopy (EDX) coupled to the scanning electron microscope.

2.4.2. DR and FTIR analysis

A UV–Vis CCD array spectrometer (BWTEK) couple to a diffuse reflectance (DR) module was used to estimate the optical band gap of the membranes at room temperature. The optical reflectance was measured in the 400–900 nm range. Then, raw DR spectra were treated using Kubelka-Munk transformation [19].

Fourier-transform spectrophotometer (FT-IR, PerkinElmer Spectrum Two) coupled to an ATR (Attenuated Total Reflectance, PerkinElmer) was used to identify the main functional groups of the membranes. For each IR measurement, the experimental conditions were 16 scans, 2 cm^{-2} of resolution, and 4000–450 cm^{-1} spectral range. The spectra were normalized to the main absorption band and baseline corrected. To assess the degree of oxidation of the semiconductor polymer, the spectra of the commercial membrane were subtracted from the modified membranes.

2.5. Mechanical properties

Mechanical properties of dry membranes were determined by stress-strain tests developed at room temperature (ca. 27 °C) using a Zwick Z010 instrument (ZwickRoell, Ulm, Germany) equipped with a 200 N static load cell. Dum-bell test pieces were obtained from each membrane according to ISO 37:2011, type 4 shape: 2.0 ± 0.1 and 35.0 ± 0.1 mm for the width in the narrow portion and overall length, respectively. At least 5 test pieces per membrane were analyzed at 10 mm min^{-1} crosshead speed using a 0.1 MPa preload until break.

2.6. Membrane fundamental properties

2.6.1. Water uptake

After the membranes pre-treatment (section 2.2.), they were washed

with some DI water and dried in vacuum oven at 60 °C at 100 mbar for 24 h (Memmert Vacuum drying oven VO). Then, weight, thickness, length, and width were measured. After that, membranes were hydrated by immersion in DI water for 24 h and water on the surface was wiped off with tissue paper to conduct the corresponding measurements. The water uptake was calculated using Eq. (1) where w_w and w_d correspond to the weight of membranes after and before soaking, respectively.

$$Water\ uptake = \frac{w_w - w_d}{w_d} \cdot 100 \quad (1)$$

2.6.2. Ion conductivity and ion exchange capacity

The through-plane ion conductivity (σ) of the membranes was measured in open circuit potential by means of Electrochemical Impedance Spectroscopy (EIS) using an AUTOLAB equipment (PGSTAT 302 N) connected to a Frequency Response Analyzer (FRA) and monitored with NOVA software in the frequency range of 10^6 Hz–1 Hz using an amplitude perturbation wave of 10 mV. The pre-treated membranes were cleaned with DI water before ion conductivity testing. σ was calculated using Eq. (2):

$$\sigma = \frac{l}{RA} \quad (2)$$

where l (cm) and A (cm^2) are the thickness and area of the membrane, respectively. R is the membrane resistance obtained by extrapolation of the low-frequency impedance curve onto the real part axis of the Nyquist plot.

The ion-exchange capacity was measured using an UV–Vis spectrophotometer (PerkinElmer, Lambda 365). Depending on the cationic or anionic characteristics of the IEM, the methodology used was different. In case of CEMs, the membrane was soaked in HCl 0.01 M. Afterwards, the membrane was cleaned with DI water to avoid acid excess on membrane surface. Then, it was left into NaCl 1 M solution. UV–Vis spectroscopy was used as quantification method. A linear regression was built with different basic-phenolphthalein (pink color) standard solutions to determine the number of displaced protons. Thus, this methodology consists of measuring the decreasing absorption produced by adding the released protons to a standard solution containing equimolar NaOH with phenolphthalein solution. This procedure let to obtain a more reliable value than the one provided by standard titration methods.

In case of AEMs, membrane was soaked in $NaNO_3$ 1 M solution, instead of HCl 0.01 M solution as in CEMs. Subsequently, the membrane was washed with DI water and then was immersed into NaCl solution. Finally, the number of displaced nitrate ions from the membranes was determined similarly to the previous one, by linear regression built with different nitrate ion solutions by using a UV–Vis spectrophotometer.

In both cases, the IEC was calculated using Eq. (3):

$$IEC = \frac{n_{displaced\ ion}}{w_d} \quad (3)$$

where $n_{displaced\ ion}$ is the number of exchanged ions from the membrane (mmol) and w_d is the weight of the dried membrane (g).

2.6.3. BP7 and TEMPOL permeability

Permeability measurements of BP7 and TEMPOL molecules, the membrane pieces of an effective area (4 cm^2) were sandwiched between two diffusion half-cells with the same volume. The left compartment was filled with 100 mM of the corresponding redox active material in NaCl 1 M solution (18 mL) and the right one was only filled with NaCl 1 M solution (18 mL). The concentration of the supporting electrolyte on the right compartment was unmodified since in our conditions osmotic pressure between the two solutions was unnecessary to minimize. The two solutions were continuously stirred to avoid the gradient concentration profile on the membrane surface. The permeation in the right compartment was checked periodically by UV–Vis spectrophotometer and calculated according to Fick's law (Eq. (4)):

$$V_B \frac{dC_B(t)}{dt} = \frac{AP}{l}(C_A - C_B(t)) \quad (4)$$

Then the permeability (P) can be calculated by Eq. (5):

$$P = \frac{V_B l}{At} \ln\left(\frac{C_A}{C_A - C_B}\right) \quad (5)$$

where P is the permeability (cm^2/s), l is the thickness of the membrane (cm), A is the cross-sectional area of the diffusion cell (cm^2), t is the time (s), C_A is the concentration of the redox active species in enrichment side (mol/cm^3) and C_B is the concentration of redox active species in the deficiency side (mol/cm^3). V_B is the volume of the deficiency side.

2.7. Static contact angle measurements

Membrane samples were cleaned with DI water and water on the surface was wiped off with tissue paper and dried overnight in a sealed desiccator attached to a glass slide for static contact angle measurements. Static water contact angle of the films was measured by using a contact angle goniometer (KSV CAM200) at room temperature. DI water was used, and the average drop size was 8 μL. Equilibrium drop contact angles were determined by taking 30 images during 15 and 30 s after the drop contacted the membrane surface. The value is obtained by the static sessile drop technique and calculated via a device-internal Young-Laplace-method fitting the images obtained. Drop contact angles were measured as the angle between the baseline of a liquid drop and the tangent at the solid-liquid boundary and the average value calculated from all the images is taken. At least three angles were measured for each sample and then their average value was calculated.

2.8. Electrochemical properties of ion exchange membranes

2.8.1. Membrane potential and apparent transport number

Membrane potential was determined by the concentration cell method based on the diffusion potential measurements across a 4 cm^2 effective area membrane which separated two NaCl 10^{-2} M and 10^{-3} M solutions, respectively, using Ag/AgCl as reference electrodes. After 2 h the membrane potential steady state was reached. Each experiment was repeated three times and the average values were calculated. Membranes were previously equilibrated in the most diluted solution for 24 h.

2.8.2. Chronopotentiometry and current-voltage curves

The cell used for chronopotentiometric measurements consisted of two symmetrical compartments between the membranes was sandwiched (4 cm^2) and two Ag/AgCl plate electrodes, obtained by oxidation in NaCl 1 M solution, to apply the desired current density. Two Ag/AgCl reference electrodes were used to measure the membrane potential drop by using Luggin capillaries. The resulting response was recorded during 240 s. Different constant currents were applied during 120 s by using AUTOLAB equipment (PGSTAT 302 N) and the membrane potential drop at the imposed current was registered.

The current-voltage curves were obtained from the steady-state polarization of chronopotentiometries at different applied currents (2–30 mA). All experiments were carried out with NaCl 0.025 M solution at room temperature and without stirring.

3. Results and discussion

The extensive use of Nafion® as ion exchange membrane has allowed to consider it as the state-of-the-art in energy storage devices both in acid and alkaline media [20,21]. Nevertheless, technical, and economic barriers related to this membrane must be still overcome. Low cost and high-performance membranes are of interest to reach new challenges for

all these devices. In this work, to improve cost barrier, some commercial membranes were selected as alternative cost-effective materials. The specific membranes tested in this work were two CEMs and two AEMs: FS-950, E-630(K), FAA-3-50 and FAA-3-PE-30, respectively, the last one containing polyethylene (PE) as a reinforcement. The membranes were properly evaluated and then modified to reduce the permeation of organic molecules.

The membrane modification proposed in this work consists on a chemical *in situ* polymerization of Py monomer by immersion method using $FeCl_3$ as initiator (see Fig. 1) [15]. This procedure has two steps. In the first step, the membrane was impregnated with the monomer covering all the surface and slipping through the holes of the membrane. In the second step, the chemical polymerization takes place immediately when soaking in the solution containing the oxidizing agent. Then, the polymer formed filled these holes that hindered the redox organic molecules crossing through the membrane while enhancing the mechanical properties of the composite membrane. Generally, the pyrrole polymerization is a sequence of oxidation, deprotonation, and cross-linking reactions by monomer oxidation. The mechanism of PPy formation is a bit controversial [22,23] but the most widely accepted is: initiation step, the coupling of two radical cations produced by the oxidizing agent (Fe^{3+}, in this case) followed by a deprotonation yielding a bipyrrole [24]. Afterwards, the obtained dimer is easily oxidized again and linked to another oxidized fragment. In this way, re-oxidation, coupling, and deprotonation are randomly occurred to form larger polymer chains in the propagation step. It is known that along the PPy chain some structures (polarons and bipolarons) are formed upon oxidation [25,26] which provide the electrical properties of this material (see Fig. S3 in SI). In general terms, synthetized PPy chains are formed by coupling of reduced (benzoid) and oxidized (quinoid) fragments as shown in Fig. 2. The oxidized/reduced ratio could give some precious information about the oxidation degree in the PPy chains attached into the membranes.

Regarding the polymerization conditions, two options were tested: one with (i) short time of Py impregnation (2 min) and Py polymerization (6 min) and the other one with (ii) long time of Py impregnation (6 min) and Py polymerization (18 min). According with obtained results, the second condition was the most efficient to reduce significantly the permeation of the redox organic molecules and therefore, this was the chosen one for the analysis provided in this paper.

3.1. Membrane characterization

3.1.1. Morphology

The surface morphology of the membranes is rather important since modify their microstructure and hence determines the transport of the ions as well as the membrane properties [27,28]. Fig. 3 shows that modified membranes were dyed with dark blue. CEMs became opaquer than AEMs. From the macroscopic point of view, every membrane exhibit quite similar and homogeneous characteristic (Fig. 3). The micro-phase morphology (both surface and cross-section) of representative membranes was characterized by scanning electron microscopy (SEM) as shown in Fig. 3(a and b). The resulting surface changed from a smooth to a rough surface without increasing the membrane thickness. Indeed, thickness after modification was checked by a micro-meter and no significant changes were observed. SEM images (Fig. 3) of the pristine

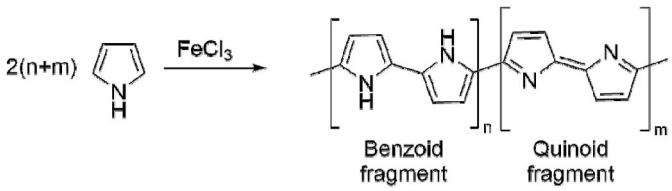

Fig. 2. Oxidative polymerization of pyrrole.

membranes show some micro-pores and cavities throughout the material in the membrane microstructure. Thus, favors the permeation of the active materials. The membrane modification proposed coats/covers not only the surface of the membrane (as demonstrated by mapping of iron and nitrogen atoms by SEM technique, Fig. 3) but the pores within the membrane, too. Therefore, the diffusion of the redox active species would be effectively reduced after the modification. The amount of pyrrole that membranes can host is limited to its absorption capacity throughout the whole thickness microstructure. Since the membranes are chemically different the distribution of the polypyrrole within the membrane must be limited to the corresponding microstructure (see Fig. 3 of SEM images) and thickness.

The elemental composition of the modified membranes was investigated by energy-dispersive X-ray spectroscopy (EDX). Qualitative analysis results show that nitrogen (as indicator of the presence of polypyrrole molecules, PPy) and iron (related to the presence of some iron occluded during the polymerization) are present throughout all membranes including the surface and inside the membranes as shown in Fig. 3(c and d). This is confirmed by the relative quantitative intensity profiles (see Table 1). The composition variations found are closely related to the type of IEM employed since a different chemical environment is found when performing the modification. This fact may explain the differences found (i) membrane colour appearance, being the CEMs the opaquest; and (ii) iron contents between CEMs and AEMs, being the last one which shows the lowest content. The higher attractive electrostatic force existing between the anionic groups in CEMs membranes and Fe^{3+} supports the results. It is worth mentioning that no significant desorption of iron atoms was observed beyond 24 h.

3.1.2. Mechanical properties

Good mechanical properties are essential to maintain the dimensional stability of membrane during working lifecycle in order to prevent catastrophic failures due to sudden breaking or tears. The mechanical properties of the membranes are presented in Table 2 and their graphical comparison are depicted in the stress-strain curve of Fig. 4. The Young's modulus, E, was determined from the slope of the initial linear part of the curve, i.e., the elastic regime of the membranes which in turn show its maximum value in the elastic limit, L_e; the ultimate tensile strength, σ_S, was found from the corresponding maximum strength in the stress-strain curve; deformation at break, ε, express the percentage of total elongation of the membrane at the fracture point referred to the initial size of the test-piece.

In general, modified membranes significantly increase their E and L_e values compared to the corresponding commercial ones but for the Young's modulus of E-630(K)-PPy, which although a slight decrease is observed, both values can be considered not significantly different. Therefore, although membranes loss deformation capacity after chemical modification as inferred from the E increasing, they maintain the elastic behavior for a higher range of applied strength. Regarding the ductility properties, PPy modified membranes show significant differences in the plastic region, too. So, even though all modified membranes reduce their maximum deformation before breaking, ε, compared to commercial ones, they can withstand higher stress before integrity loss or breaking as given by σ_S values.

Therefore, it can be concluded that PPy-modified membranes increase their rigidity while decrease their deformation, i.e., PPy modification has a reinforcement effect on original membranes improving their mechanical strength by PPy crosslinking in the original pores of commercial membranes. Considering the pursuit AORFB application of these membranes where they will perform their functionality under static conditions, the PPy incorporation is a positive factor as it enhances the membrane physical stability and integrity along time. It is possible to contextualize these results by comparing with those of the Nafion® membrane which constitutes the reference in energy storage electrochemical devices, currently. So, although mechanical properties of Nafion® are highly dependent of hydration level, PPy-membranes

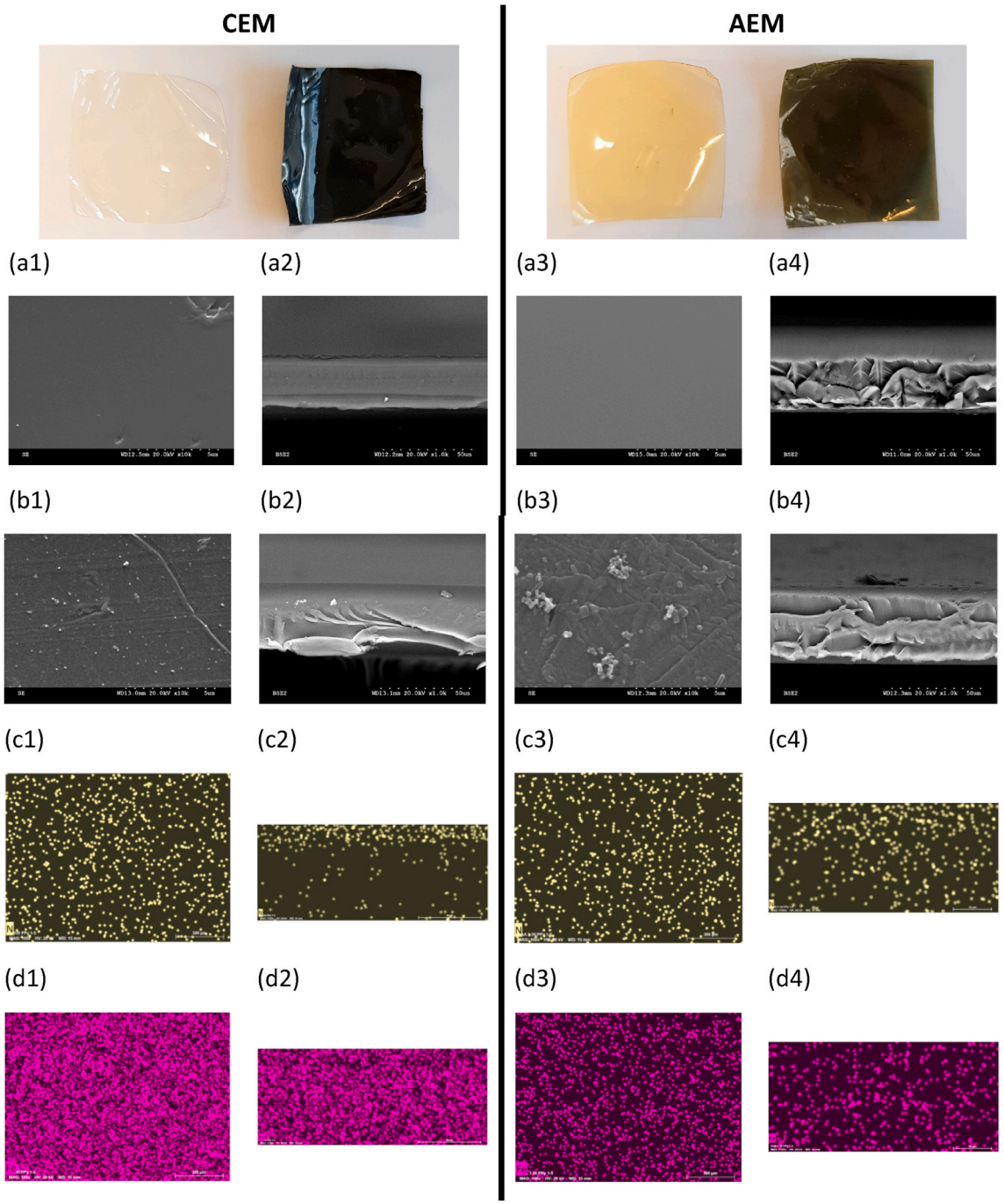

Fig. 3. Membrane morphology of representative membranes. CEM: E-630(K) (left) *vs* E-630(K)-PPy (right). AEM: FAA-3-50 (left) *vs* FAA-3-50-PPy (right). (a) pristine, (b) modified membrane, (c) SEM/EDX mapping of nitrogen and (d) SEM/EDX mapping of iron. Subscript 1 and 3 correspond to surface membrane images. Subscript 2 and 4 correspond to cross-section membrane images.

Table 1
Surface EDX analysis of the modified membranes.

Samples	Membrane type	Iron content (%)	Nitrogen content (%)
FS-950-PPy	CEM	5.30	10.34
E-630(K)-PPy	CEM	3.46	2.24
FAA-3-50-PPy	AEM	0.16	1.91
FAA-3-PE-30-PPy	AEM	1.27	5.08

Table 2
Mechanical properties of the commercial and modified membranes in dried conditions.

Samples	E (MPa)	σ_S (MPa)	L_e (MPa)	ε (%)
FS-950	399.6 ± 56.2	16.81 ± 3.4	9.9 ± 3.1	≈18
FS-950-PPy	768.8 ± 42.7	23.3 ± 1.3	17.0 ± 0.3	≈12
E-630(K)	1097.0 ± 64.0	24.1 ± 0.6	19.3 ± 1.1	≈8
E-630(K)-PPy	1031.4 ± 44.5	25.6 ± 1.9	23.9 ± 1.7	≈6
FAA-3-50	634.2 ± 37.5	18.1 ± 1.3	15.3 ± 0.3	≈6
FAA-3-50-PPy	1093.5 ± 77.1	34.2 ± 3.7	26.0 ± 1.3	≈4
FAA-3-PE-30	492.2 ± 78.5	21.8 ± 4.3	11.5 ± 0.7	≈11
FAA-3-PE-30-PPy	797.8 ± 77.6	31.9 ± 5.1	17.4 ± 2.5	≈7

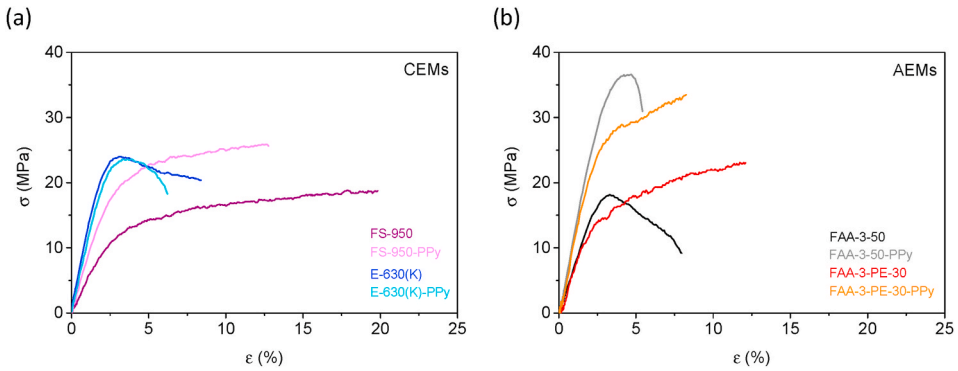

Fig. 4. Mechanical tensile strength before and after the PPy modification of (a) CEMs and (b) AEMs.

exhibit significant improved mechanical strength [28] but, in other hand, more brittle behavior, too.

3.1.3. FTIR and DR analysis

The functional characterization of the commercial IEMs was carried out by FTIR spectroscopy as shown in Fig. 5. The peak intensities around 1460 (–CH_2 δ), 1303 (– CH_3 δ) and 2900 cm^{-1} (C–H st) are found in both AEMs suggesting a similar monomer composition. The presence of these bands imply hydrocarbon polymeric chains. The absorption band around 3400 cm^{-1} can be assigned to the presence of –NH group and/or the membrane humidity. Absorption peak that arises at a frequency below 3000 cm^{-1} in FAA-3-50 and more intense, in FAA-3-PE-30 is due to the stretching vibration of the –C–H– bond. Such slightly differences are probably caused by distinction of incorporating polyethylene (PE) as a reinforcement in the membrane. Absorption peaks at around 1601 cm^{-1} is probably due to –C═C– groups. Additionally, the absorption band around 1188 cm^{-1} (C–N) suggests that ion fixed groups attached on the polymeric chains could be ammonium-type groups.

In case of CEMs, both membranes FS-950 and E-630(K) showed similar composition to N117 membrane since characteristic peaks at frequencies around 1203-1147, 1078, 624 and 510 cm^{-1} were attributed to CF_2, $–SO_3H$, C–H and C–F groups [29]. As well as the absorption peak around 3400 cm^{-1} which is due to the presence of –OH group. By contrast, the absorption peaks found in E-630(K) below 3000 cm^{-1} and between 1595 and 1470 cm^{-1} revealed that E-630(K) membrane is not fully fluorinated polymer membrane as is the case of FS-950 (Nafion®-like). According to FTIR spectra all the characteristic peaks are present in the membrane, revealing the presence of sulfonic-type functional groups in CEMs.

The infrared absorption spectra of the modified membranes show noticeable differences compared to pristine membranes at regions around 1700–1520 cm^{-1} and 990–890 cm^{-1} (highlighted in squares). Besides, in case of FAA-3-PE-30 overlapped bands around 2950–2840 cm^{-1} and 740–640 cm^{-1} were observed after the membrane modification. There is a strong relationship between the oxidation degree and the observed vibrational modes with the properties of the semiconductor polymer and therefore the membrane properties.

The different oxidation degree can be explained by the polaron – bipolaron model structures which is widely used to explain the properties of conducting polymers [25]. These PPy oxidized species are formed upon doping (oxidation by $FeCl_3$) which generates excess holes and therefore, creates a *p*-type semiconductor. The assignment of the

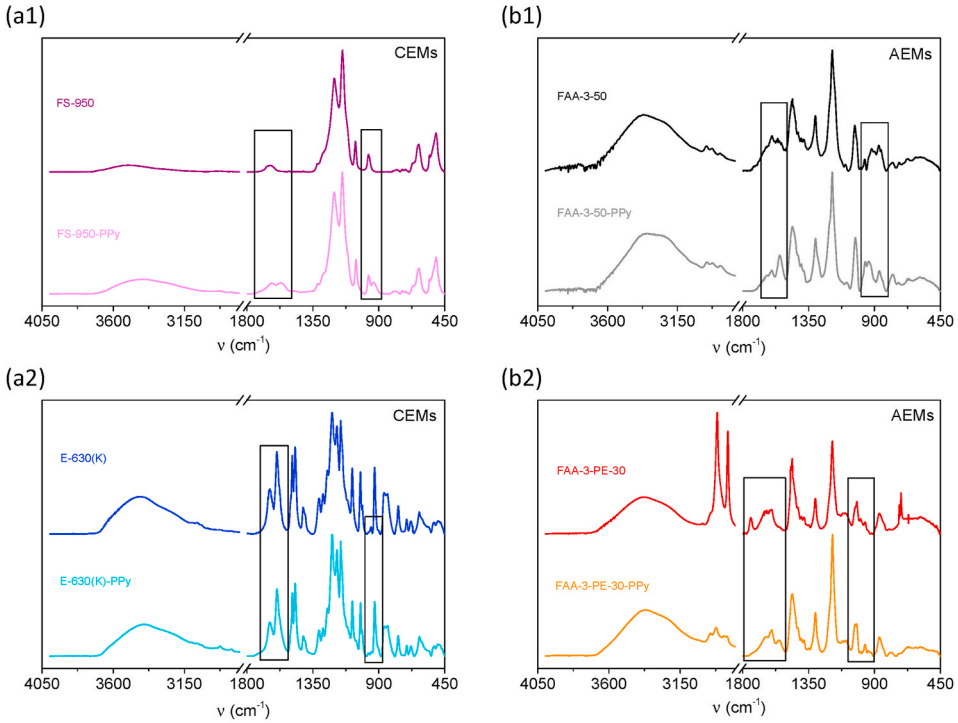

Fig. 5. FTIR spectra before and after the PPy modification of (a1–a2) CEMs and (b1–b2) AEMs.

vibrational bands of polarons and bipolarons [30,31] are well known and arises around 1620 cm^{-1} (quinoid fragment) whereas the reduced form of PPy arises around 1560 cm^{-1} (benzoid fragment). Both bands correspond to $\nu_{c=c}$ assignment. Additionally, bands around 925 cm^{-1} (quinoid fragment) and 990 cm^{-1} (benzoid fragment) correspond to ν_{c-H} assignment and are well observed in Fig. 5. By integration of these band areas, it is possible to determine the oxidation degree of the corresponding PPy-based membranes (see Table 3). FS-950-PPy and FAA-3-PE-30-PPy showed high level of oxidation being the FAA-3-PE-30-PPy the most oxidized (≈72% of oxidation) whereas in case of FAA-3-50-PPy was the lowest (≈37%). In case of E-630(K)-PPy was not possible to estimate due to overlapping of bands. These values were calculated by the deconvolution of the bands (quinoid and benzoid fragments) between the modified and pristine membrane spectra. This estimation led us to confirm the presence of different polymeric chains along the different materials which may modify the physicochemical properties of the membrane composite (see section 3.3). However, higher oxidation degree does not necessarily imply larger amount of positive charges of PPy, since they evolve towards the formation of neutral double bonds and therefore, lose their electronic properties [32].

Diffuse reflectance (DR) allows to determine the neutral – polaron – bipolaron transitions in the modified membranes as shown in Table 3 and Fig. 6. The different band gap energies from DR show the coexistence of the vibrational bands associated to quinoid and benzoid fragments, also confirming the presence of different PPy structures in the polymeric chain at a given oxidation degree (see also Fig. S4 of the DR raw spectra in SI). According to literature [25], high band gap transitions (above 3.2 eV) indicate lower oxidation degree whereas lower values (below 1.5 eV) point to elevated oxidation degree. This is related to the concentration of positive charges (polarons and bipolarons) along the PPy chains that provide the material *p*-type semiconductor characteristics. However, a concentration excess of positive charges decreases the electrical performance due to chemical instability and they evolve to degradation. According to the values obtained, transitions between 1.75 and 2.85 eV suggest low concentration of positive charges in the modified membranes. However, according to the estimated values of oxidation degree went the opposite trend. This apparent contradiction can be explained by the loss in electronic conductivity due to degradation of the PPy even more in case of FAA-3-PE-30-PPy. Nevertheless, as a general conclusion no electronic conductor properties would be expected in any modified membrane according to the high electronic transitions observed. In fact, electronic transitions below 1 eV are typical in a good semiconductor material.

3.2. Membrane permeability

The crossover of the redox active species through the membranes is detrimental to the RFB operation, leading to self-discharge and progressive capacity decay of the battery. Preventing these transport phenomena would enable more effective battery performance and longer lifecycle. Thus, the modification performed in this work is a suggestive strategy improve the durability and performance of the battery. Methyl viologen and TEMPO derivatives, such as BP7 and TEMPOL in the anolyte and catholyte, respectively, both display remarkable electrochemical reversibility (see their chemical structure in Fig. S6 in SI).

In this work, modified membranes were tested in terms of BP7 and TEMPOL permeability. As shown in Fig. S7 in SI, permeability of BP7 and TEMPOL was obtained from the slope of linear relationship of $\ln\left(\frac{C_A}{C_A-C_B}\right)$ *vs.* time of the corresponding organic electroactive material. Data in Table 4 shows that the permeability effect was successfully reduced with all tested membranes when performing the modification. In case of TEMPOL molecule crossover is reduced three order of magnitude in best case with FAA-3-50-PPy membrane; however, permeability reduction was so significant for BP7 molecule. BP7 molecule (Fig. S6a) has two positive charges whereas TEMPOL (Fig. S6b) is uncharged under the experimental conditions. Taking into consideration the charge properties of organic species and the exchangeable sites of the membranes, one may suppose an influence in terms of coulombic interactions. Surprisingly the common Donnan effect, which is usually observed in this kind of systems, is not as significant in charged compounds (BP7) as in the case of neutral ones, i.e. TEMPOL molecule. Additionally, higher concentration of the redox active species and the hydrodynamic effect in RFB devices would certainly increase the given permeability values. Thus, crossover reduction across the membrane is essential and the methodology here described reduces the permeation of the active species by filling the pores and cavities of the pristine membranes hindering the diffusional channels of the membrane.

Table 3
Estimated values obtained from FTIR (degree of oxidation) and DR (absorption maximum and band gap energies) spectra of the modified membranes.

Samples	Membrane type	Estimated oxidation degree (%)	Absorption max. energies (eV)	Estimated band gap (eV)
FS-950-PPy	CEM	60	1.8 and 2.5	1.75 and 2.40
E-630(K)-PPy	CEM	–	2.0 and 2.7	1.75 and 2.50
FAA-3-50-PPy	AEM	37	2.1 and 2.9	1.75 and 2.35
FAA-3-PE-30-PPy	AEM	72	2.8 and 3.2	2.45 and 2.85

3.3. Membrane properties

The differences found in physicochemical properties between pristine and modified membranes are listed in Table 5. It should be noted that membrane thickness shown in table below was measured as received. Usually, membranes would absorb water depending on the hydrophilicity of the backbone polymer and the nature of the ionic groups attached in the polymeric chains. On one hand, larger amounts of water uptake (WU) would compromise the mechanical properties of the membrane materials [33,34]. On the other hand, lower WU would increase the resistivity of the material altering the energy density of the battery device.

Non-modified membranes presented similar water uptake values (15.6–19.6%); these would be affordable for battery operation. By contrast, water uptake after modification significantly decreases. This is concomitant with the values obtained in contact angle measurements in Table 5. The water contact angle measurements were obtained according to Young's equation (Eq. (6)) where θ is the contact angle, γ^{SV}, γ^{SL} and γ^{LV} are the solid, solid-liquid and liquid surface free energies, respectively. This methodology confirmed the presence of PPy in the membranes surface. After the modification, contact angles increased from 70.0°–93.0°–80.1°–96.5° (see Fig. S8 in SI). Thus, the surface of pristine membranes became more hydrophobic since water diffusion inside the membrane was hindered by the presence of PPy molecules.

It is worth mentioning that FAA-3-PE-30 possess two different faces, one non-containing PE as a reinforcement and the opposite containing the PE reinforcement. Once analyzed both faces, the membrane area without reinforcement reduces significantly their hydrophilicity whereas in the other side containing the PE remains unaltered maybe due to a bad interaction between the PE and PPy.

$$\gamma^{SV} = \gamma^{SL} + \gamma^{LV}\cos(\theta) \tag{6}$$

Ion conductivity is a crucial membrane parameter since directly affects the energy density of RFBs. Depending on the nature of the membrane, it will exchange positive or negative ions and the ion mobility of such species will affect the specific resistivity of the material. In this work, CEMs and AEMs exchange sodium and chloride ions, respectively.

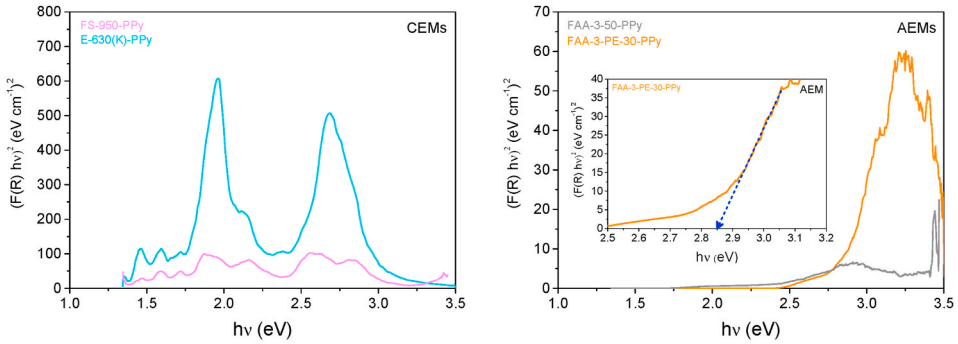

Fig. 6. DR spectra of modified membranes. (a) CEMs and (b) AEMs. Detail of GAP calculation for FAA-3-PE-30-PPy membrane is provided (see Fig. S5 in SI for the rest of GAP calculations).

Table 4
BP7 and TEMPOL permeability of commercial and modified membranes. All membranes were evaluated in NaCl 1 M and tested at r.t.

Samples	Membrane type	BP7 permeability (x 10^{10} cm^{2}s^{-1})	TEMPOL permeability (x 10^{10} cm^{2}s^{-1})
FS-950	CEM	2.49	96.0
FS-950-PPy		2.49	30.6
E-630(K)	CEM	122.0	1.21
E-630(K)-PPy		1.45	0.97
FAA-3-50	AEM	1.26	192.0
FAA-3-50-PPy		1.26	0.63
FAA-3-PE-30	AEM	5.41	68.8
FAA-3-PE-30-PPy		1.39	0.62

Table 5
Physicochemical properties of pristine and modified membranes.

Samples	Thickness (μm)	WU (%)	Contact angle (°)	Ion conductivity[c] (mS cm^{-1})	IEC (mmol g^{-1})
FS-950	52.0	15.8	84.8 ± 2.0	2.2	1.5
FS-950-PPy		3.2	93.4 ± 1.0	5.3	0.4
E-630(K)	34.0	19.6	70.2 ± 2.0	2.6	1.1
E-630(K)-PPy		6.1	81.4 ± 2.2	3.5	0.9
FAA-3-50	45.0	15.6	85.3 ± 3.9	1.1	1.9
FAA-3-50-PPy		6.6	96.5 ± 0.9	3.8	2.3
FAA-3-PE-30	23.0	17.1	70.0 ± 2.8[a]/81.0 ± 2.2[b]	0.3	1.1
FAA-3-PE-30-PPy		0.8	80.1 ± 2.0[a]/80.4 ± 2.7[b]	1.5	2.0

[a] Face area non-containing PE as a reinforcement.
[b] Face membrane area containing PE as a reinforcement.
[c] Conductivity measurements were performed in a two-chambers cell set-up under flowing wetted air at 30 °C.

For both CEMs, FS-950 and E-630(K), sodium conductivity σ_{Na^+}, is quite similar, 2.2 mS cm^{-1} and 2.6 mS cm^{-1}, respectively. However, AEMs (which are chemically similar) chloride conductivity σ_{Cl^-}, is significantly lower for FAA-3-PE-30 (0.3 mS cm^{-1}) in comparison with FAA-3-50 (1.1 mS cm^{-1}). This result can be explained in terms of the PE reinforcement presence in FAA-3-PE-30 membrane. Reinforcement plays an important role when considering ion conductivity of the membrane materials since implies the increasing of non-conducting regions in the modified material, although on the other hand it improves the mechanical properties. Concerning about membrane modification, one may suppose that the incorporation of a polymeric material into the membrane would decrease the membrane conductivity since the ion conductivity is mainly given by the electrolyte absorbed in the pores and cavities in the microstructure of membranes. Nevertheless, all membranes showed an increase of ion conductivity once the modification was performed (from 0.3 to 2.6 to 1.5–5.3 mS cm^{-1}) despite of filling partially those pores and cavities responsible for their conductivity. This fact was attributed to the different structural PPy molecules formed into the ion exchange membrane (confirmed by the infrared and diffuse reflectance). It is known that PPy displays a slight ion conductivity at a given oxidation state, higher as the oxidation levels increases [16]. In this sense, the holes along the PPy chains (polarons and bipolarons) acts as conducting centres and favours the mobility of counter-ions present in the system (chloride ions, in this case). Additionally, a pristine and modified membranes (FS-950 vs. FS-950-PPy e.g.) were dried at 60 °C during 24 h and the conductivity measured at these conditions was $1.6{\cdot}10^{-4}$ and $1.7{\cdot}10^{-4}$ mS cm^{-1}, respectively. At this scenario, the conductivity obtained is not due to ion mobility effects. Therefore, the values obtained belong to electronic contribution and as it can be observed, the modification in the modified membranes is unsignificant in terms of electronic contribution. Thereby, the differences in ionic conductivity observed (see Table 5) in our experimental conditions are attributed to the PPy and/or some iron attached to the membranes. In this context, PPy contribution has a beneficial impact in membrane conductivity. However, the conductivity obtained was without a continuous supply of electrolyte through the pores and cavities of the membrane. When analyzing the through plane conductivity of membranes by means of a flow battery cell, we ensure a continuous supply of electrolyte into the pores and cavities of membranes through a constant flow. By comparing the conductivity obtained from the two-chambers and flow battery devices, pristine membranes showed a significant increase from 0.54 to 4.39 mS cm^{-1}, respectively, whereas the conductivity increase in modified membranes is just 1.6 times from 0.85 to 1.33 mS cm^{-1}, respectively. Both membranes increased their conductivity due to the greater supply of the electrolyte solution through their microstructure. However, in case of modified membranes the conductivity is lower since their pores and cavities are partially filled with PPy. Thereby, the incorporation of PPy as an ionomer in modified membranes have a different contribution depending on the cell conditions. However, the modification proposed let us diminish the cross-mixing of the organic redox active species (see Table 4) that could lead to significant losses of capacity and final performance in battery systems to long terms of battery operational mode.

The ion-exchange capacity (IEC) provides information regarding the amount of ion groups that possess the material, which is an important factor related to the conductivity and therefore, with the transport properties of the membranes. The highest IEC values were obtained with the thickest membranes, anionic (FAA-3-50 with 1.9 mmol g^{-1}) and cationic (FS-950 with 1.5 mmol g^{-1}) whereas the thinnest ones show

1.1 mmol g^{-1} for both FAA-3-PE-30 and E-630(K). Additionally, the discrepancies found in membranes of the same nature after modification could be probably due to the different thickness, which is related to the amount of PPy that membranes can host in their microstructure. All these materials are chemically and microstructurally different and exhibit transport properties, too. Nevertheless, it is worth mentioning that AEMs with highly values of IEC usually become unstable depending on the pH media and tend to degrade since they have more active sites for degradation pathways [35,36]. The values of IEC obtained are in good agreement with the battery purposes working at neutral pH.

However, after PPy modification, IEC changes differently according to type of ion exchange membrane. In CEMs the IEC decreased down to 0.4 and 0.9 mmol g^{-1}, for FS-950-PPy and E-630(K)-PPy, respectively, whereas in AEMs the IEC values were increased up to 2.3 and 2.0 mmol g^{-1}, for FAA-3-50-PPy and FAA-3-PE-30-PPy, respectively. This fact is in agreement with spectroscopic results obtained by DR since show how different oxidized PPy species in our membranes are present. So, negatively charged membranes (CEMs) may interact with oxidized PPy molecules decreasing the IEC by electrostatic interaction and generating a sort of bipolar membrane because PPy contains positive charged structures; in the other side, in positively charged membranes (AEMs) the increasing of IEC could be related to the incorporation of more positive charges along the polymeric matrix of the membrane during polymerization. It is worth mentioning that the Fe^{3+} ion kept in the membranes after polymerization may influence since can interact electrostatically as well.

3.4. Membrane permselectivity

The coulombic and energy efficiency of electrochemical devices based in the use of ionic exchange membranes are significant dependent of the charge carriers mobility across the membrane. In this study, sodium and chloride ions are the charge carriers of the RFB. Transport number considers the fraction of total current carried by counter-ions crossing through ion exchange membranes. The apparent transport number has been obtained in this work by potentiometric method. A static concentration potential is generated from the inter diffusion of the counter-ions across the ion exchange membranes using a diffusional cell, measuring the potential difference originated in the vicinity of the membrane (see experimental section 2.8.1). The value can be calculated by Eq. (7) where a_1 and a_2 are the mean activities of electrolyte solutions.

$$E_m = \left(2t^m_{app,i} - 1\right)\frac{RT}{nF}\ln\left(\frac{a_1}{a_2}\right) \tag{7}$$

Indeed, not all the membrane materials have the same ability to exchange the counter-ions and this requires evaluation. This analysis can be performed looking at the ion selectivity which can be obtained by the permselectivity (Ps) parameter. Ps provides information regarding the ease of counter-ion migration through this kind of systems concerning about the number of exchangeable sites and the effectiveness of the process. Ps can be calculated using Eq. (8):

$$Ps = \frac{t^m_{app,i} - t^s_i}{1 - t^s_i} \tag{8}$$

where t^s_i is the transport number of the counter-ion in free solution at infinite diluted conditions. One may suppose that the effect of PPy growth into the membrane would restrict the movement of bulkier ions across the membranes. However, it was evidenced that the transport number and the permselectivity of the membranes before and after PPy modification has a negligible influence in ion exchangeable effectiveness and thus in ion selectivity (see Fig. 7).

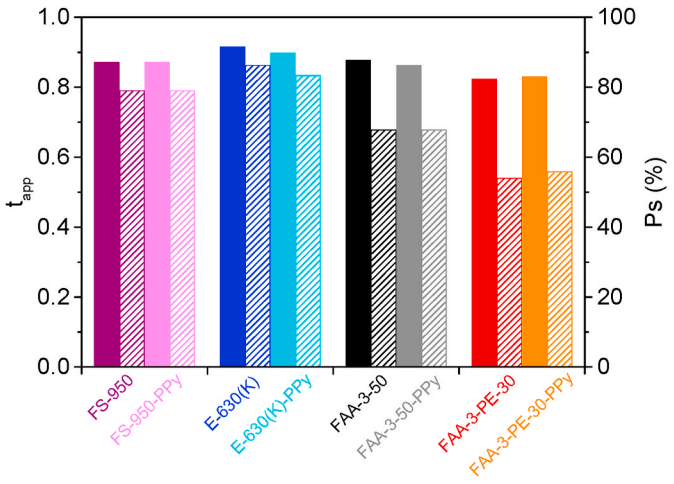

Fig. 7. Apparent transport number (filled columns) and permselectivity (dashed columns) of membranes.

3.5. Membrane microstructure

Despite chemical homogeneous polymer in ion exchange membranes can be obtained, it is known that there is some micro-heterogeneity in ion exchange groups distribution [37,38]. Then, two different type of IEMs can be distinguished: homogeneous and heterogeneous, in which ion exchange groups are attached to the matrix polymer regularly (hydrophilic part) or irregularly distributed over the material containing inert regions (hydrophobic regions), respectively. Then, a membrane consists of ion conducting and non-conducting regions. Therefore, from the microstructure point of view some mechanisms for ion motion should be considered in the membrane phase. In this work, we wanted to evaluate how transfer processes occur in the membranes before and after modification and study the corresponding effects by means of chronopotentiometry. It is necessary to consider that even the so-called homogeneous membranes, such as Nafion®, present non-conductive regions due to the microheterogeneities found at sub-microscopic scale [39].

3.5.1. Determination of membrane conducting area: effect of heterogeneity

When a direct current is applied through a membrane the polarization concentration can be developed and if this is up to the point that the counter-ion concentration at the membrane depleting surface approach to zero an increase of E_m is shown. The chronopotentiometric curves (E_m *vs* time) obtained in NaCl 0.025 M solution by applying current densities from 2 to 30 mA cm^{-2} for both pristine and modified membranes are shown in Fig. S9 in SI. The curve has distinct four parts as shown in Fig. 8). At t = 0 no current is applied and solution concentrations at both sides are equal being the measured potential zero. In region 1, at fixed current density, the potential drop corresponds to the ohmic resistance of membrane-electrolyte system. In region 2, the membrane potential slightly increases up to an inflection point (region 3). The inflection point is known as transition time (τ) and it is related to the surface electrolyte concentration near the membrane/solution interface that drops to zero because the membrane is permselective to the counter-ions and thereby reaches its maximum potential differences. τ can be obtained by plotting the first derivative of the curve with respect to time. It only occurs at current densities above the limiting current density. However, τ decreases when applying current densities larger than limiting current density. After inflection point, alternative mass transfer mechanisms (mainly convection) take place. Finally, the potential growth decreases to zero and stabilize with time (region 4). The regions 5 and 6 are due to after switching off the current and the subsequent relaxation of the system, respectively.

The transition time is determined from the maximum of the deriva-

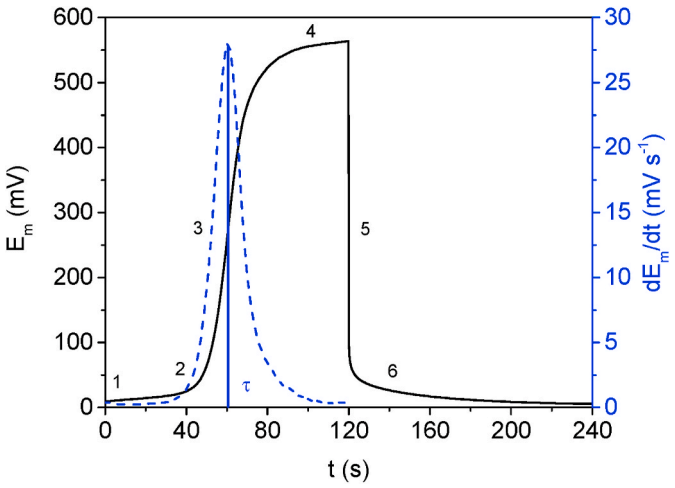

Fig. 8. Characteristic shape of chronopotentiometry curve obtained (black line) at a given current density above the limiting current density for a representative membrane (FAA-3-PE-30-PPy at 3.000 mA cm^{-2}) and its derivative (dashed blue line) to obtain τ value. (For interpretation of the references to colour in this figure legend, the reader is referred to the Web version of this article.)

tive of the E_m *vs* t obtained from Fig. 8. Transition time is given by Sand's equation (Eq. (9)) and its mathematical model assumes that diffusion of ions takes place homogeneously in one dimension and in the absence of any forced or natural convection in the membrane surface.

$$i\tau^{1/2} = \frac{(\pi D_s)^{1/2}}{2} \frac{C_0 z_i F}{t_i^m - t_i^s} \tag{9}$$

According to this equation: D_s is the diffusion coefficient of NaCl; the transport numbers of the counter ion in the membrane and solution are defined as t_i^m and t_i^s, respectively; C_0 concentration in the bulk; z_i is the charge of the counter-ion; i is the current density; and F is the Faraday constant. According to Sand's equation, this expression implies $i\tau^{1/2}$ constant values at different current densities at a given membrane transport number. In this work, it was evidenced that permselectivity of membranes was approximately the same when performing the modification (see Fig. 6). However, the experimental results shown in Fig. 9 (a1–a2) showed some differences in $i\tau^{1/2}$ values between pristine and modified membranes suggesting another effect on microstructure.

Choi et al. [38] implemented a method to estimate the fraction of conductive region (ε) of IEMs by chronopotentiometry. Based in a non-ideal behaviour of Sand's model, this method would assess differences in ion conducting and non-conducting regions. Thus, Sand's equation depends on the transition time at a given applied current density and can be expressed for a semi-infinite diffusion phenomenon considering no influence of forced or natural convection and thus an unlimited growth of the diffusion layer of the membrane. By incorporating the ε parameter, information regarding to the conducting area of the ion exchange membranes can be obtained by using Eq. (10).

$$\tau = \varepsilon^2 \frac{\pi D_s}{4} \left(\frac{z_i F}{t_i^m - t_i^s} \right)^2 \left(\frac{C_0}{i} \right)^2 \tag{10}$$

By plotting the obtained transition times (see Fig. 9 (b1–b2)), τ, as a function of $\left(\frac{C_0}{i}\right)^2$, for currents above limiting current, the conducting region of membranes can be determined from the slope of the straight line using Eq. (10) and considering a sodium and chloride transport number of 0.385 and 0.615 in the bulk solution [40], respectively, and a sodium chloride diffusion coefficient value of $1.61 \cdot 10^{-5}$ cm^2 s^{-1} [41] which were found in literature. The fractions of conducting region were calculated and listed in Table 6.

Based on the obtained results, most of the pristine membranes showed higher contents of non-conducting regions but for E-630(K) membrane which was about 95%. After PPy modification, the conducting regions were markedly decreased except of FAA-3-PE-30 which

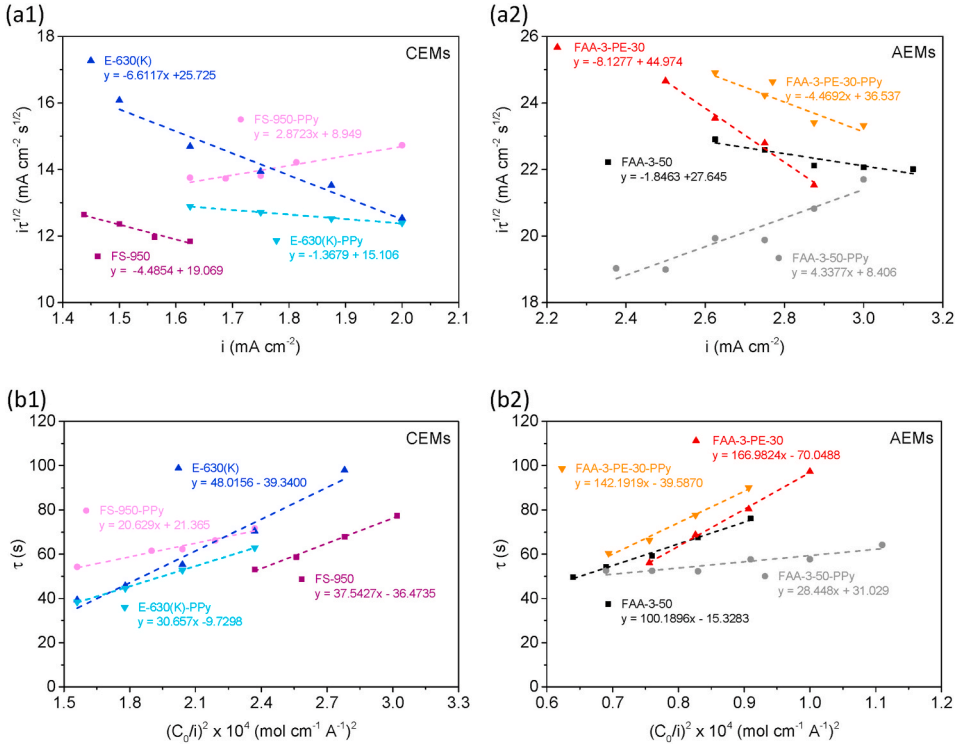

Fig. 9. The $i\tau^{1/2}$ values for different (a1) CEMs and (a2) AEMs as a function of current density supplied. Transition time, τ, as a function of $\left(\frac{C_0}{i}\right)^2$ for different (b1) CEMs and (b2) AEMs in contact with a NaCl 0.025 M solution.

Table 6
Values and fractions of conducting region of membranes before and after the PPy modification.

Samples	slope x 10^4 s·(A·cm)^2 mol^{-2}	ε
FS-950	37.54	0.77
FS-950-PPy	20.63	0.57
E-630(K)	48.02	0.95
E-630(K)-PPy	30.66	0.73
FAA-3-50	100.19	0.67
FAA-3-50-PPy	28,45	0.34
FAA-3-PE-30	166.98	0.69
FAA-3-PE-30-PPy	142.19	0.66

remained practically unaltered. Probably, the PE layer that contains this membrane may have had some influence during polymerization. All these effects are in agreement with SEM/EDX and permeability data, since membrane surface changed and the PPy film deposited into the membrane hindered the diffusion of the redox active species while increasing the heterogeneity of the membrane surface at microstructure level.

3.5.2. *Effect of membrane heterogeneity on limiting current densities*

Simultaneously to the fraction of conducting regions, information regarding to the limiting current density can be obtained from chronopotentiograms. The limiting current is the region where concentration polarization becomes predominant and the ions motion over the membrane surface are limited by diffusion. Polarization curves are built from the steady-state membrane potential in the chronopotentiograms. Three main regions can be distinguished: an ohmic region (region 1) where the system obeys the Omh's law; followed by a plateau, which defines the value of current density (region 2), and a subsequent, increase of the current density (region 3). This increase of current is due to several effects such as possible water splitting, electro-convection and formation of space charges in the polarization layer [42]. Fig. 10 shows the obtained polarization curves of membranes. It was observed that in region 1, the PPy modified membranes showed less ohmic resistance when compared with the corresponding pristine ones especially in case of FAA-3-PE-30-PPy membrane. This data suits with the through-plane ion conductivity values obtained. In general trends, two different electrochemical behaviors were observed depending on the type of ion exchange membrane. On one hand, the *plateau* length of CEMs was slightly shortened when performing the modification especially the E-630 (K)-PPy which was practically non-existent. In fact, the *plateau* length is a measure of the energy requirements to eliminate the diffusion boundary layer [43]. Therefore, the lower the *plateau* length, the lower the stability on the boundary conditions and this may affect long-term exchange efficiency since the double layer is continuously destroying leading to convective processes. And on the other hand, the *plateau* length of AEMs was slightly extended when performing the modification suggesting a greater double layer stability on boundary conditions. The limiting current density (LCD) was determined by the intersection of the two slopes belonging to the ohmic and *plateau* regions. The LCD value can be calculated using Eq. (11).

$$i_{lim} = \frac{z_i F C_0 D_s}{\delta(t_i^m - t_i^s)} \tag{11}$$

where i_{lim} is a limiting current density and δ is a diffusion boundary layer thickness. However, since membranes are not homogeneous, the heterogeneity on surface promotes higher local current densities through the regions with good conductivity. Therefore, the ion concentration over the membrane surface at these regions is lower in comparison with the ones at homogeneous membrane surface at a given current. Consequently, tangential diffusion may occur in well-conducting regions to counterbalance that effect [40]. The diffusion boundary layer thickness (δ) is influenced by the hydrodynamic state of the electrolyte solution, thus stirring-less solution was performed during analysis. Diffusion boundary layer thickness was calculated according to the fraction of conducting regions following Eq. (11). The superficial and local LCD as

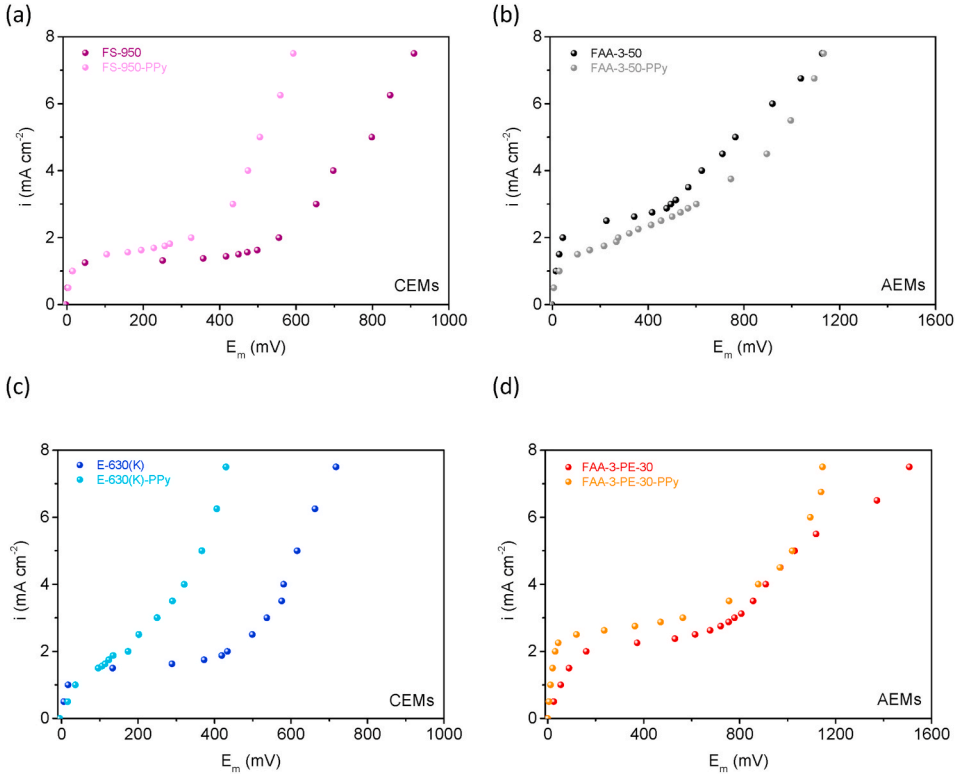

Fig. 10. Polarization curves before and after the modification of ion exchange membranes soaked in NaCl 0.025 M solution. (a) FS-950 *vs*. FS-950-PPy, (b) FAA-3-50 *vs*. FAA-3-50-PPy, (c) E-630(K) *vs*. E-630(K)-PPy and (d) FAA-3-PE-30 *vs*. FAA-3-PE-30-PPy.

Table 7
Limiting current densities (LCD) and diffusion boundary layer of different ion exchange membranes before and after the PPy modification.

Samples	Superficial LCD (mA cm^{-2})	Local LCD (mA cm^{-2})	δ (μm)
FS-950	1.18	1.53	522.4
FS-950-PPy	1.23	2.16	370.0
E-630(K)	1.37	1.44	534.9
E-630(K)-PPy	1.07	1.60	523.2
FAA-3-50	2.29	3.42	435.1
FAA-3-50-PPy	1.45	1.79	882.1
FAA-3-PE-30	1.94	2.81	664.5
FAA-3-PE-30-PPy	2.23	3.23	559.3

well as δ for each membrane are reported in Table 7. As a result, greater limiting current density values were obtained in case of CEMs and the reciprocal of diffusion boundary layer thickness, just the opposite for AEMs but for FAA-3-PE-30-PPy. In this membrane, the high degree of oxidation and the reinforcement of PE could have an influence on transport properties.

Thus, this analysis led us to confirm a different chemical behavior at microstructure level increasing the non-conducting regions while keeping the effectiveness of the ion exchange after PPy modification. These results demonstrate that the microheterogeneity has an impact on limiting boundary conditions depending on the type of ion exchange membrane being the AEMs the most stable to long-term exchange.

4. Conclusions

In this work, we have studied the effect of pyrrole polymerization on four different, commercially available ion exchange membranes, two cationic (CEMs) and two anionic (AEMs). From a physicochemical point of view, this report presents a fundamental approach to improve the performance of low-cost membranes used in aqueous organic redox flow battery application. The symbiosis of electrochemical and novel spectroscopic investigation, coupled to the PPy modification is an excellent approach to pursuit better understanding of these materials. In particular, our studies show that pyrrole polymerization successfully reduces the permeation of two redox active organic molecules, viologen derivative BP7 and TEMPOL, and gives a plausible explanation of the role of PPy in IEMs. SEM/EDX mapping analysis confirmed the presence of PPy on the membrane surface as well as inside it, blocking diffusion channels of redox active species. In the perspective to use these modified membranes as separators for AORFB applications, the effect of doping membranes with a well-known *p*-type semiconductor will not have electrical effect in battery application.

The modification performed has an impact on chemical and electrochemical properties of ion exchange membranes. While the effectiveness of exchange of ions was not altered, IEC was decreased in the case of CEMs, whereas in AEMs it was increased due to the slightly different concentration of positive charge PPy structures into the membranes that interact with the chemical structure. The electrochemical response of modified ion exchange membranes further highlighted the effect of using CEMs or AEMs on membrane transport properties in relation to the membrane characteristics. CEMs showed lower diffusion double layer stability against modification strategy.

As a conclusion, this approach to membrane modification with polypyrrole translates into lower crossover in ion exchange membranes, enabling cost-effective AORFBs for grid scale energy storage. We believe this work will inspire future studies in ion motion, as well as other chemical details of the interacting membrane and solution.

Author statement

I.Salmeron-Sanchez: Conceptualization, Methodology, Validation, Investigation, Writing – original draft, Writing – review & editing and Visualization. J. Asenjo-Pascual: Conceptualization, Methodology, Validation, Investigation, Writing – review & editing and Visualization. J.C. Pérez-Flores: Methodology, Validation, Writing – review & editing. P. Mauleón: Writing – review & editing and Funding acquisition. J.R. Avilés-Moreno: Conceptualization, Methodology, Validation, Writing – review & editing, Supervision and Funding acquisition. P. Ocón: Conceptualization, Methodology, Validation, Resources, Writing – review & editing, Supervision and Funding acquisition. All authors gave approval to the final version of the manuscript.

Declaration of competing interest

The authors declare that they have no known competing financial interests or personal relationships that could have appeared to influence the work reported in this paper.

Acknowledgements

This work has been funded by the European Union under the HIGREEW project, Affordable High-performance Green Redox Flow batteries (Grant agreement no. 875613). H2020: LC-BAT-4-2019.

Appendix A. Supplementary data

Supplementary data to this article can be found online at https://doi.org/10.1016/j.memsci.2021.120020.

References

[1] K. Lourenssen, J. Williams, F. Ahmadpour, R. Clemmer, S. Tasnim, Vanadium redox flow batteries: a comprehensive review, J. Energy Storage. 25 (2019) 100844–100861, https://doi.org/10.1016/j.est.2019.100844.
[2] X. Yan, Z. Dong, M. Di, L. Hu, C. Zhang, Y. Pan, N. Zhang, X. Jiang, X. Wu, J. Wang, G. He, A highly proton-conductive and vanadium-rejected long-side-chain sulfonated polybenzimidazole membrane for redox flow battery, J. Membr. Sci. 596 (2020) 117616–117624, https://doi.org/10.1016/j.memsci.2019.117616.
[3] T.P. Vaid, M.S. Sanford, An organic super-electron-donor as a high energy density negative electrolyte for nonaqueous flow batteries, Chem. Commun. 55 (2019) 11037–11040, https://doi.org/10.1039/c9cc06080d.
[4] T. Liu, X. Wei, Z. Nie, V. Sprenkle, W. Wang, A total organic aqueous redox flow battery employing a low cost and sustainable methyl viologen anolyte and 4-HO-TEMPO catholyte, Adv. Energy Mater. 6 (2016) 1501449–1501457, https://doi.org/10.1002/aenm.201501449.
[5] Z. Tang, R. Svoboda, J.S. Lawton, D.S. Aaron, A.B. Papandrew, T.A. Zawodzinski, Composition and conductivity of membranes equilibrated with solutions of sulfuric acid and vanadyl sulfate, J. Electrochem. Soc. 160 (2013) F1040–F1047, https://doi.org/10.1149/2.083309jes.
[6] C. Chu, W. Lee, Y. Kwon, The effect of additives on the performance of aqueous organic redox flow battery using quinoxaline and ferrocyanide redox couple, Kor. Chem. Eng. Res. 57 (2019) 847–852, https://doi.org/10.9713/kcer.2019.57.6.847.
[7] B. Jiang, L. Wu, L. Yu, X. Qiu, J. Xi, A comparative study of Nafion series membranes for vanadium redox flow batteries, J. Membr. Sci. 510 (2016) 18–26, https://doi.org/10.1016/j.memsci.2016.03.007.
[8] N. Ramaswamy, N. Hakim, S. Mukerjee, Degradation mechanism study of perfluorinated proton exchange membrane under fuel cell operating conditions, Electrochim. Acta 53 (2008) 3279–3295, https://doi.org/10.1016/j.electacta.2007.11.010.
[9] J.S. Lawton, A. Jones, T. Zawodzinski, Concentration dependence of VO 2+ crossover of nafion for vanadium redox flow batteries, J. Electrochem. Soc. 160 (2013), https://doi.org/10.1149/2.004306jes. A697–A702.
[10] T. Luo, S. Abdu, M. Wessling, Selectivity of ion exchange membranes: a review, J. Membr. Sci. 555 (2018) 429–454, https://doi.org/10.1016/j.memsci.2018.03.051.
[11] N. Kononenko, V. Nikonenko, D. Grande, C. Larchet, L. Dammak, M. Fomenko, Y. Volfkovich, Porous structure of ion exchange membranes investigated by various techniques, Adv. Colloid Interface Sci. 246 (2017) 196–216, https://doi.org/10.1016/j.cis.2017.05.007.
[12] B. Schwenzer, J. Zhang, S. Kim, L. Li, J. Liu, Z. Yang, Membrane development for vanadium redox flow batteries, ChemSusChem 4 (2011) 1388–1406, https://doi.org/10.1002/cssc.201100068.
[13] J. Sheng, A. Mukhopadhyay, W. Wang, H. Zhu, Recent advances in the selective membrane for aqueous redox flow batteries, Mater. Today Nano. 7 (2019) 100044–100053, https://doi.org/10.1016/j.mtnano.2019.100044.
[14] Q. Luo, H. Zhang, J. Chen, P. Qian, Y. Zhai, Modification of Nafion membrane using interfacial polymerization for vanadium redox flow battery applications, J. Membr. Sci. 311 (2008) 98–103, https://doi.org/10.1016/j.memsci.2007.11.055.

[15] J. Zeng, C. Jiang, Y. Wang, J. Chen, S. Zhu, B. Zhao, R. Wang, Studies on polypyrrole modified nafion membrane for vanadium redox flow battery, Electrochem. Commun. 10 (2008) 372–375, https://doi.org/10.1016/j.elecom.2007.12.025.
[16] C. Ehrenbeck, K. Jüttner, Ion conductivity and permselectivity measurements of polypyrrole membranes at variable states of oxidation, Electrochim. Acta 41 (1996) 1815–1823, https://doi.org/10.1016/0013-4686(95)00500-5.
[17] M. Yamaura, T. Hagiwara, K. Iwata, Enhancement of electrical conductivity of polypyrrole film by stretching: counter ion effect, Synth. Met. 26 (1988) 209–224, https://doi.org/10.1016/0379-6779(88)90238-X.
[18] S. Melnikov, S. Shkirskaya, Transport properties of bilayer and multilayer surface-modified ion-exchange membranes, J. Membr. Sci. 590 (2019) 117272–117285, https://doi.org/10.1016/j.memsci.2019.117272.
[19] H.G. Hecht, Interpretation of diffuse reflectance spectra, J Res Natl Bur Stand Sect A Phys Chem 80 (1976) 567–583, https://doi.org/10.6028/jres.080A.056.
[20] W. Lee, G. Park, Y. Kwon, Alkaline aqueous organic redox flow batteries of high energy and power densities using mixed naphthoquinone derivatives, Chem. Eng. J. 386 (2020) 123985–123995, https://doi.org/10.1016/j.cej.2019.123985.
[21] L. Hoober-Burkhardt, S. Krishnamoorthy, B. Yang, A. Murali, A. Nirmalchandar, G. K.S. Prakash, S.R. Narayanan, A new Michael-reaction-resistant benzoquinone for aqueous organic redox flow batteries, J. Electrochem. Soc. 164 (2017), https://doi.org/10.1149/2.0351704jes. A600–A607.
[22] E. Garfias-García, M. Romero-Romo, M.T. Ramírez-Silva, J. Morales, M. Palomar-Pardavé, Mechanism and kinetics of the electrochemical formation of polypyrrole under forced convection conditions, J. Electroanal. Chem. 613 (2008) 67–79, https://doi.org/10.1016/j.jelechem.2007.10.013.
[23] S. Sadki, P. Schottland, N. Brodie, G. Sabouraud, The mechanisms of pyrrole electropolymerization, Chem. Soc. Rev. 29 (2000) 283–293, https://doi.org/10.1039/a807124a.
[24] C.P. Andrieux, P. Audebert, P. Hapiot, J.M. Savéant, Identification of the first steps of the electrochemical polymerization of pyrroles by means of fast potential step techniques, J. Phys. Chem. 95 (1991) 10158–10164, https://doi.org/10.1021/j100177a096.
[25] J.L. Bredas, J.C. Scott, K. Yakushi, G.B. Street, Polarons and bipolarons in polypyrrole: evolution of the band structure and optical spectrum upon doping, Phys. Rev. B 30 (1984) 1023–1025, https://doi.org/10.1103/PhysRevB.30.1023.
[26] S. Ghosh, G.A. Bowmaker, R.P. Cooney, J.M. Seakins, Infrared and Raman spectroscopic studies of the electrochemical oxidative degradation of polypyrrole, Synth. Met. 95 (1998) 63–67, https://doi.org/10.1016/s0379-6779(98)00034-4.
[27] T. Sata, R. Izuo, K. Takata, Modification of the transport properties of ion exchange membranes. IX. Layer formation on a cation exchange membrane by acid-amide, and transport properties of the resulting membrane, J. Membr. Sci. 45 (1989) 197–208, https://doi.org/10.1016/j.memsci.2019.117272.
[28] C. Feng, Y. Li, K. Qu, Z. Zhang, P. He, Mechanical behavior of a hydrated perfluorosulfonic acid membrane at meso and nano scales, RSC Adv. 9 (2019) 9594–9603, https://doi.org/10.1039/C9RA00745H.
[29] R.K. Singh, K. Kunimatsu, K. Miyatake, T. Tsuneda, Experimental and theoretical infrared spectroscopic study on hydrated nafion membrane, Macromolecules 49 (2016) 6621–6629, https://doi.org/10.1021/acs.macromol.6b00999.
[30] M.J.L. Santos, A.G. Brolo, E.M. Girotto, Study of polaron and bipolaron states in polypyrrole by in situ Raman spectroelectrochemistry, Electrochim. Acta 52 (2007) 6141–6145, https://doi.org/10.1016/j.electacta.2007.03.070.
[31] Y.C. Liu, B.J. Hwang, Identification of oxidized polypyrrole on Raman spectrum, Synth. Met. 113 (2000) 203–207, https://doi.org/10.1016/S0379-6779(00)00188-0.
[32] J. Stejskal, M. Trchová, P. Bober, Z. Morávková, D. Kopecký, M. Vrňata, J. Prokeš, M. Varga, E. Watzlová, Polypyrrole salts and bases: superior conductivity of nanotubes and their stability towards the loss of conductivity by deprotonation, RSC Adv. 6 (2016) 88382–88391, https://doi.org/10.1039/c6ra19461c.
[33] S. Kundu, L.C. Simon, M. Fowler, S. Grot, Mechanical properties of Nafion™ electrolyte membranes under hydrated conditions, Polymer (Guildf) 46 (2005) 11707–11715, https://doi.org/10.1016/j.polymer.2005.09.059.
[34] M.A. Vandiver, B.R. Caire, T.P. Pandey, Y. Li, S. Seifert, A. Kusoglu, D.M. Knauss, A.M. Herring, M.W. Liberatore, Effect of hydration on the mechanical properties and ion conduction in a polyethylene-b-poly(vinylbenzyl trimethylammonium) anion exchange membrane, J. Membr. Sci. 497 (2016) 67–76, https://doi.org/10.1016/j.memsci.2015.09.034.
[35] J.A. Vega, C. Chartier, W.E. Mustain, Effect of hydroxide and carbonate alkaline media on anion exchange membranes, J. Power Sources 195 (2010) 7176–7180, https://doi.org/10.1016/j.jpowsour.2010.05.030.
[36] K.D. Kreuer, P. Jannasch, A practical method for measuring the ion exchange capacity decrease of hydroxide exchange membranes during intrinsic degradation, J. Power Sources 375 (2018) 361–366, https://doi.org/10.1016/j.jpowsour.2017.07.106.
[37] C. Selvey, H. Reiss, Ion transport in inhomogeneous ion exchange membranes, J. Membr. Sci. 23 (1985) 11–27, https://doi.org/10.1016/S0376-7388(00)83131-2.
[38] J.H. Choi, S.H. Kim, S.H. Moon, Heterogeneity of ion-exchange membranes: the effects of membrane heterogeneity on transport properties, J. Colloid Interface Sci. 241 (2001) 120–126, https://doi.org/10.1006/jcis.2001.7710.
[39] W.Y. Hsu, T.D. Gierke, Ion transport and clustering in nafion perfluorinated membranes, J. Membr. Sci. 13 (1983) 307–326, https://doi.org/10.1016/S0376-7388(00)81563-X.
[40] X.T. Le, P. Viel, D.P. Tran, F. Grisotto, S. Palacin, Surface homogeneity of anion exchange membranes: a chronopotentiometric study in the overlimiting current range, J. Phys. Chem. B 113 (2009) 5829–5836, https://doi.org/10.1021/jp900138v.
[41] N. Pismenskaia, P. Sistat, P. Huguet, V. Nikonenko, G. Pourcelly, Chronopotentiometry applied to the study of ion transfer through anion exchange membranes, J. Membr. Sci. 228 (2004) 65–76, https://doi.org/10.1016/j.memsci.2003.09.012.
[42] F. Maletzki, H.W. Rösler, E. Staude, Ion transfer across electrodialysis membranes in the overlimiting current range: stationary voltage current characteristics and current noise power spectra under different conditions of free convection, J. Membr. Sci. 71 (1992) 105–116, https://doi.org/10.1016/0376-7388(92)85010-G.
[43] L. Marder, E.M. Ortega Navarro, V. Pérez-Herranz, A.M. Bernardes, J.Z. Ferreira, Evaluation of transition metals transport properties through a cation-exchange membrane by chronopotentiometry, J. Membr. Sci. 284 (2006) 267–275, https://doi.org/10.1016/j.memsci.2006.07.039.